International Journal of Multiphase Flow 36 (2010) 769–779

Contents lists available at ScienceDirect

International Journal of Multiphase Flow

journal homepage: www.elsevier.com/locate/ijmulflow

Fundamentals of migrating multi-block lattice Boltzmann model for immiscible mixtures in 2D geometries

Hassan Farhat [a], Joon Sang Lee [b,*]

[a] Department of Mechanical Engineering, Wayne State University, Detroit, MI, USA
[b] Department of Mechanical Engineering, Yonsei University, Seoul, Republic of Korea

ARTICLE INFO

Article history:
Received 25 November 2009
Received in revised form 6 June 2010
Accepted 6 July 2010

Keywords:
Multi-block
Grid refinement
Multiphase flows
Immiscible mixtures
Gunstensen model

ABSTRACT

This paper proposes an extension scheme for the application of the single phase multi-block lattice Boltzmann method (LBM) to the multiphase Gunstensen model, in which the grid is refined in a specific part of the domain where a fluid–fluid interface evolves, and the refined grid is free to migrate with the suspended phase in the flow direction. The method is applicable to single and multiphase flows, and it was demonstrated by simulating a benchmark single phase flow around a 2D asymmetrically placed cylinder in a channel and for investigating the shear lift of 2D neutrally buoyant drop in a parabolic flow.

1. Introduction

The lattice Boltzmann method (LBM) has been successfully used for solving variety of fluid flow problems. However the LBM uses equidistant lattice spacing since the propagation step is dependent on discrete velocity direction vectors with constant magnitudes. This dictates the use of a structured grid, which leads in the case of insufficient lattice spacing to some distorted results. To remedy this problem and for undergoing grid independence test a finer grid is usually used. This increases the computational expense and degrades the LBM efficiency.

Several models were introduced to improve the LBM quality, and to save computational time (Fillipova and Hanel, 1998; He and Doolen, 1997; He et al., 1996; Huang et al., 2006; Imamura et al., 2005; Kandhai et al., 2000; Li et al., 2005; Lin and Lai, 2000; Liu et al., 2009; Shu et al., 2001; van der Sman, 2004; Yu and Girimaji, 2006; Yu et al., 2002), especially for problems related to turbulent flows, and flows in complex geometries such as porous media. These models can be classified either by the method used: interpolation, hybrid LBM, and grid refinement, or by the nature of the grid: structured and unstructured grid.

Interpolation method was first suggested by He et al. (1996), who noted that the density distribution function was continuous in the physical space therefore it was possible to define its value on a non-uniform grid through interpolation. The method was further extended by Shu et al. (2001), and Li et al. (2005) who used Taylor series expansion and least square respectively, to evaluate the distribution function rather than using a direct interpolation. Imamura et al. (2005) used local time step on non-uniform grid to accelerate the solution since each grid point had its own time step based on the local advection time stability condition.

Hybrid LBM for unstructured grid combined the LBM with some traditional CFD tools like finite difference, finite volume, and finite element. Hybrid LBM benefited from the LBM stability, which resulted from the use of the particle velocity in the model instead of the macroscopic velocity. This guaranteed the satisfaction of the Courant–Friedrichs–Lewy (CFL) stability condition, while maintained the accuracy and efficiency of the traditional CFD tools (Kandhai et al., 2000; Huang et al., 2006).

An interesting unstructured LBM model was proposed by van der Sman (2004) in which no interpolation was required, since particle velocity in this model was different for different lattice sites. This led to the elimination of the undesired numerical diffusion caused by the interpolation step.

Grid refinement methods were designed for structured grids in which a finer mesh was needed in parts of the domain characterized by complex geometry, and where higher accuracy was required. Fillipova and Hanel (1998) introduced the first model which passed information from the post-collision distribution functions between the coarse and the fine grids. The transfer of data maintained continuous viscosity and Reynolds number throughout the domain. The model also handled very well complex geometries by specially treating curved boundaries. Lin and Lai

* Corresponding author.
E-mail address: joonlee@yonsei.ac.kr (J.S. Lee).

0301-9322/$ - see front matter © 2010 Elsevier Ltd. All rights reserved.
doi:10.1016/j.ijmultiphaseflow.2010.07.001

(2000) proposed a composite block-structured LBM in which a coarse grid covered the whole domain and only areas of interest were patched with a fine grid blocks. This method did not need time interpolation, because solutions on both grids were at the same time level. Yu et al. (2002) suggested a very efficient multi-block method in which the fine and the coarse grids did not overlap throughout the domain, and information transfer occurred only at the grid interface. This method was later expanded to 3D by Yu and Girimaji (2006) and will be revisited in Section 2.

Multiphase and multi-component flows were not as extensively studied with respect to grid refinement, as single phase flows. The peculiarity of the multiphase flows is due to the movement and deformation of the suspended phase. This hampers the use of pre-set grid refinement techniques since the area of interest is not stationary. Tolke et al. (2006) proved in their Gunstensen based LBM, that the interface was distorted relative to the magnitude of the capillary forces, when the fluid interface was allowed to pass through the grid interface of different preset fixed grids. They also indicated using a mathematical model that the useful grid level in such cases was very restricted. Thus they resorted to the use of an adaptive grid method, in which the physical interface was always discretized on the finest grid level. Ozawa and Tanahashi (2005) presented a model for multiphase flow, with an adaptive unstructured grid in which cubic interpolation was used with the volume/area coordinates method for the streaming step and moving least-square method for the collision step. The mesh was refined based on a number density threshold using the bisection algorithm.

The present work's objective is to provide a simple algorithm, aiming at saving considerable computational time in simulations where local grid refinement is required, and especially applicable to multiphase flows with highly deformable interface. To avoid the difficulties faced by Tolke et al. (2006), and to maintain a relatively simple approach using standard structured grid LBM, a Gunstensen based model combined with the multi-block method of Yu et al. (2002), is proposed here. The difference in the proposed model lies in that, a fine grid block covers the entire fluid interface and migrates with it, so that the physical interface does not cross the grid interface. This is performed by tracking the mass center or the average velocity of the suspended fluid, which acts as a trigger to impose node type exchange at the grid interfaces in a way that does not alter the physical properties of the various fluids. The node type exchange occurs without time lag during the propagation step in the coarse block. The grid interface is always imposed where a single phase exists. This broadens the potential applicability of the algorithm to other LBM models such as the Shan and Chen and the free energy models.

This paper is organized as follows: Section 2 reviews LBM, the Gunstensen model, and the migrating multi-block LBM. Section 3 includes the simulation of a benchmark single phase flow around an asymmetrically placed cylinder in a channel, and a multiphase simulation of the lift of neutrally buoyant drop in a parabolic flow. Section 4 is for the conclusion and future work.

2. Numerical method

2.1. Standard LBM and the Gunstensen model

The Bhatnagar–Gross–Krook (BGK) lattice Boltzmann method is used extensively as an alternative computational technique for solving variety of fluid problems. The D2Q9 isothermal, single-relaxation model is based on Boltzmann kinetic equation:

$$\frac{df}{dt}+\boldsymbol{\xi}\cdot\nabla f=-\frac{1}{\lambda}(f-f^{eq}) \tag{1}$$

f is density distribution function, ξ is macroscopic velocity, and λ is relaxation time in the physical space. Eq. (1) is first discretized in the velocity space using finite set of velocities $\{\xi_i\}$ and this leads to the following:

$$\frac{df_i}{dt}+\boldsymbol{\xi}_i\cdot\nabla f_i=-\frac{1}{\lambda}(f_i-f_i^{eq}) \tag{2}$$

The equivalent set of Cartesian velocities in the D2Q9 LBGK has the following direction vectors:

$$\begin{aligned} &c_0=(0.0)\\ &c_i=\sqrt{2}c\left(\cos\left[(i-1)\frac{\pi}{4}\right],\sin\left[(i-1)\frac{\pi}{4}\right]\right)\quad \text{for } i=2,4,6,8\\ &c_i=c\left(\cos\left[(i-1)\frac{\pi}{4}\right],\sin\left[(i-1)\frac{\pi}{4}\right]\right)\quad \text{for } i=1,3,5,7 \end{aligned} \tag{3}$$

where $c=\frac{\delta_x}{\delta_t}$ is the lattice velocity, δ_x is lattice space, and δ_t is the lattice time step. The equilibrium distribution function is expressed as:

$$f_i^{eq}=\rho\omega_i\left[1+\frac{3}{c^2}\boldsymbol{c}_i\cdot\boldsymbol{u}+\frac{9}{2c^4}(\boldsymbol{c}_i\cdot\boldsymbol{u})^2-\frac{3}{2c^2}\boldsymbol{u}\cdot\boldsymbol{u}\right] \tag{4}$$

where ω_i are the weighting constants for the various lattice links:

$$\begin{aligned} &\omega_i=\frac{4}{9}\quad \text{for } i=0\\ &\omega_i=\frac{1}{36}\quad \text{for } i=2,4,6,8\\ &\omega_i=\frac{1}{9}\quad \text{for } i=1,3,5,7 \end{aligned} \tag{5}$$

$\boldsymbol{u}$ and ρ are the macroscopic velocity and density, respectively. The macroscopic density and momentum are calculated from the distribution function by a simple arithmetic summation:

$$\rho=\sum_{i=0}^{8}f_i=\sum_{i=0}^{8}f_i^{eq} \tag{6}$$

$$\rho\boldsymbol{u}=\sum_{i=1}^{8}\boldsymbol{c}_i f_i=\sum_{i=1}^{8}\boldsymbol{c}_i f_i^{eq} \tag{7}$$

Eq. (2) is further discretized in space and time to yield:

$$f_i(\boldsymbol{x}+\boldsymbol{c}_i\delta_t,t+\delta_t)-f_i(\boldsymbol{x},t)=-\frac{1}{\tau}[f_i(\boldsymbol{x},t)-f_i^{eq}(\boldsymbol{x})] \tag{8}$$

where $\tau=\lambda/\delta_t$ is the lattice relaxation time. The speed of sound in this model is $c_s=c/\sqrt{3}$ and the pressure is calculated directly from the equation of state for ideal gas $p=\rho c_s^2$. The kinematic viscosity is a function of the relaxation time and it is expressed as follows:

$$\nu=(\tau-0.5)c_s^2\delta_t \tag{9}$$

Using Chapman–Enskog expansion the BGK can recover the Navier–Stokes equations to a second order accuracy for low Mach numbers and slow Density variation (Chen et al., 1992; Guo et al., 2000). In classical BGK model the square lattice length δ_x and time scale δ_t are taken as unity. The same will be used in the proposed model.

The Gunstensen model for binary mixtures introduces a red and a blue fluid density distribution functions $R_i(\boldsymbol{x},t)$ and $B_i(\boldsymbol{x},t)$. The total density distribution function is the sum of the two functions:

$$f_i(\boldsymbol{x},t)=R_i(\boldsymbol{x},t)+B_i(\boldsymbol{x},t) \tag{10}$$

To track the interface of the fluid–fluid interface, a phase field is defined as follows:

$$\rho^N(\boldsymbol{x},t)=\frac{R(\boldsymbol{x},t)-B(\boldsymbol{x},t)}{R(\boldsymbol{x},t)+B(\boldsymbol{x},t)} \tag{11}$$

where N is the direction normal to the interface. The macroscopic densities for the red and blue fluids are calculated by the following relationships:

$$R(\boldsymbol{x},t)=\sum_{i=0}^{8}R_i(\boldsymbol{x},t) \tag{12}$$

$$B(\boldsymbol{x},t)=\sum_{i=0}^{8}B_i(\boldsymbol{x},t) \tag{13}$$

During initialization of the LBM the directional densities are calculated by $R_i = \rho_R\omega_i$, $B_i = \rho_B\omega_i$ where ρ_R and ρ_B are constant initial densities. In this model unit density ratio was used leading to $\rho_R = \rho_B$. After initialization the various directional densities are calculated by the segregation rules.

The two fluids can have different viscosities, hence different relaxation times. The interface is made of a fluid mix with an effective viscosity calculated by the following equation:

$$v_{eff}=(\tau_{eff}-0.5)c_s^2\delta_t=\left(\frac{R}{R+B}\right)v_R+\left(\frac{B}{R+B}\right)v_B \tag{14}$$

To create interfacial tension and segregate the two immiscible fluids, the Gunstensen LBM uses two-step collision rules (Gunstensen et al., 1991; Lishchuk et al., 2003; Reis and Philip, 2007). The main collision step is the first step of the collision rules:

$$\widehat{f}_i(\boldsymbol{x},t+\delta_t)=f_i(\boldsymbol{x},t)-\frac{1}{\tau}[f_i(x,t)-f_i^{eq}(\rho,\rho\boldsymbol{u}^*)]+\phi_i(\boldsymbol{x}) \tag{15}$$

where $\widehat{f}_i$ refers to post-collision distribution function, and $\phi_i(x)$ is a source term used for inducing the desired interfacial tension and for applying an external force.

The creation of a pressure step through the interface is executed by the method of Lishchuk et al. (2003) using the following force:

$$\boldsymbol{F}(\boldsymbol{x})=-\frac{1}{2}\alpha K\nabla\rho^N \tag{16}$$

where α is a surface tension parameter, K is the curvature, and $\nabla\rho^N$ is a phase field gradient which has a nonzero value only at the interface. An accurate relationship between the source term and the macroscopic force was initially suggested by Guo et al. (2002). The same was later used by Halliday et al. (2007) for spatially varying force as follows:

$$\phi_i(\boldsymbol{x})=\omega_i\left(1-\frac{1}{2\tau}\right)[3(\boldsymbol{c}_i-\boldsymbol{u}^*)+9(\boldsymbol{c}_i\cdot\boldsymbol{u}^*)\boldsymbol{c}_i]\cdot\boldsymbol{F}(\boldsymbol{x}) \tag{17}$$

where the corrected macroscopic velocity is calculated by:

$$\boldsymbol{u}^*=\frac{1}{\rho}\left[\sum_{i=1}^{8}f_i\boldsymbol{c}_i+\frac{1}{2}\boldsymbol{F}(\boldsymbol{x})\right] \tag{18}$$

Meanwhile for a constant body force the following simpler relation is used:

$$\phi_i=\omega_i\frac{1}{k_2}\boldsymbol{F}\cdot\boldsymbol{c}_i \tag{19}$$

where $k_2\delta_{\alpha\beta} = \sum_i\omega_i c_{i\alpha}c_{i\beta}$ and for the 2D LBM $k_2 = 1/3$, $\boldsymbol{F}$ is a constant macroscopic force.

The next collision step is the segregation process which is achieved by imposing zero diffusivity of one color into the other. Numerical algorithm for the segregation step was used in the model of Gunstensen et al. (1991). A local color gradient is identified as follows:

$$\boldsymbol{G}(\boldsymbol{x},t)=\sum_{ij}\boldsymbol{c}_i(R_j(\boldsymbol{x}+\boldsymbol{c}_i,t)-B_j(\boldsymbol{x}+\boldsymbol{c}_i,t)) \tag{20}$$

A local color flux is calculated by the following formula:

$$\boldsymbol{J}=\sum_i\boldsymbol{c}_i(R_i(\boldsymbol{x},t)-B_i(\boldsymbol{x},t)) \tag{21}$$

The segregation step is achieved by forcing the local color flux to align with the direction of the local color gradient. Thus the colored distribution functions at the interface are redistributed such that $-\boldsymbol{J}\cdot\boldsymbol{G}$ is maximized and the following constraints are applied:

$$\begin{aligned}&\sum_i\widehat{R}_i(\boldsymbol{x},t)=R(\boldsymbol{x},t)\\&\widehat{B}_i(\boldsymbol{x},t)=\widehat{f}_i(\boldsymbol{x},t)-\widehat{R}_i(\boldsymbol{x},t)\end{aligned} \tag{22}$$

D'Ortona et al. (1995) proposed a formulaic approach, which was later modified slightly and implemented by Halliday et al. (2007) using the following relationship:

$$\begin{aligned}\widehat{R}_i(\boldsymbol{x},t+\delta_t)&=\frac{R}{R+B}\widehat{f}_i(\boldsymbol{x},t+\delta_t)+\beta\frac{RB}{R+B}\omega_i\cos(\theta_f-\theta_i)|\boldsymbol{c}_i|\\\widehat{B}_i(\boldsymbol{x},t+\delta_t)&=\frac{B}{R+B}\widehat{f}_i(\boldsymbol{x},t+\delta_t)-\beta\frac{RB}{R+B}\omega_i\cos(\theta_f-\theta_i)|\boldsymbol{c}_i|\end{aligned} \tag{23}$$

where θ_f and θ_i are the polar angle of the color field, and the angle of the velocity link respectively, β is the segregation parameter. $\widehat{R}_i, \widehat{B}_i$ refer to the post-collision post-segregation red and blue functions respectively. The numerical segregation provides a sharp interface desired for many applications, especially when the size of the suspended fluid is relatively small. Hence this method is used in this work together with Eq. (19) for the perturbation of the interface prior to the segregation step.

After segregation the two fluids are propagated separately by the following formulae:

$$\begin{aligned}R_i(\boldsymbol{x}+\boldsymbol{c}_i\delta_t,t+\delta_t)&=\widehat{R}_i(\boldsymbol{x},\boldsymbol{t}+\delta_t)\\B_i(\boldsymbol{x}+\boldsymbol{c}_i\delta_t,t+\delta_t)&=\widehat{B}_i(\boldsymbol{x},\boldsymbol{t}+\delta_t)\end{aligned} \tag{24}$$

The macroscopic observables are then calculated using Eqs. (6) and (7). The individual fluid densities are calculated Eqs. (12) and (13). For detailed information on the Gunstensen LBM we refer the reader to the work of (Dupin et al., 2003, 2005, 2007; Halliday et al., 2007).

2.2. Migrating multi-block LBM

The following is a brief description of Yu et al. (2002) multi-block LBM tailored for this work domain, in which the width is much smaller than the length. The domain shown in Fig. 1 consists of three blocks: an upstream coarse block, a fine block, and a downstream coarse block. The ratio of the lattice spacing between the fine and coarse blocks is defined as:

$$m=\frac{\delta_x^c}{\delta_x^f} \tag{25}$$

δ_x^c and δ_x^f are the lattice spacing in the coarse and the fine grid blocks, respectively. To maintain the same viscosity, and therefore the same Reynolds number in the various blocks, the relaxation times have to satisfy the following equality:

$$\tau_f=\frac{1}{2}+m(\tau_c-0.5) \tag{26}$$

Each grid interface consists of overlapping two sets of coarse and fine nodes with one additional set of fine nodes filling in the gap as shown in Fig. 1. The transfer of the post-collision distribution functions $\widehat{f}_i^f \rightleftarrows \widehat{f}_i^c$ between the different grids occurs before the streaming step. To maintain the same lattice velocity $(\delta_x^c/\delta_t^c = \delta_x^f/\delta_t^f)$ between the various grids, the time step ratio is the same as the spatial ratio $(m = \delta_x^c/\delta_x^f = \delta_t^c/\delta_t^f)$. After one collision step in the coarse block a transfer of data $(\widehat{f}_i^f \leftarrow \widehat{f}_i^c)$ is required at the indicated locations in Fig. 1 by the following rule:

$$\widehat{f}_i^f=f_i^{eq,c}+\frac{\tau_f-1}{m(\tau_c-1)}[\widehat{f}_i^c-f_i^{eq,c}] \tag{27}$$

After m collision steps in the fine grid a transfer of data $(\widehat{f}_i^f \rightarrow \widehat{f}_i^c)$ is required at the indicated locations in Fig. 1 by the following formula:

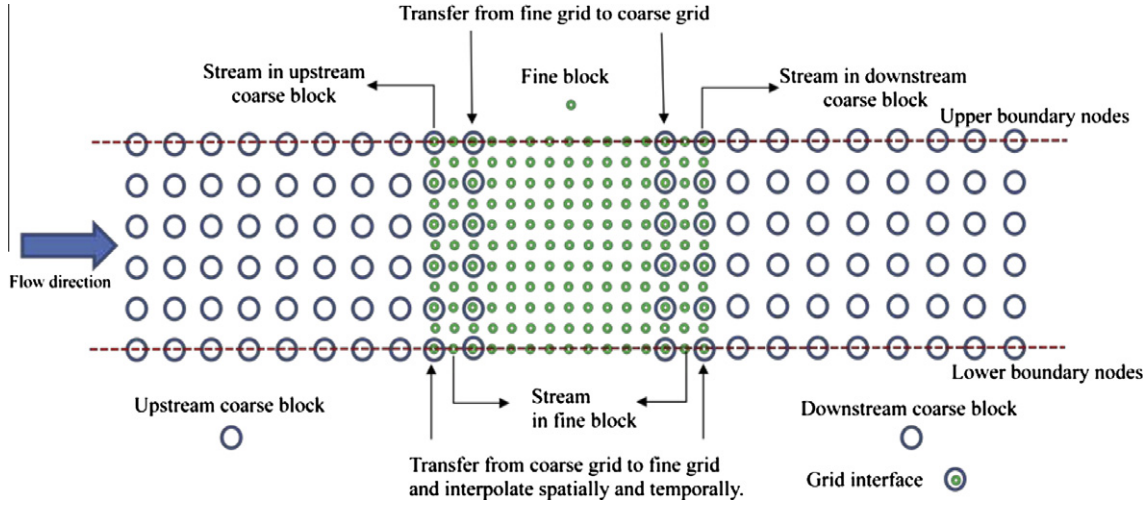

Fig. 1. Illustration of the standard multi-block LBM domain as it pertains to the single component flow simulation of this work.

$$\widehat{f_i^c} = f_i^{eq,f} + m\frac{\tau_c - 1}{(\tau_f - 1)}[\widehat{f_i^f} - f_i^{eq,f}] \tag{28}$$

A symmetric cubic spline interpolation is required for calculating $\widehat{f_i^f}$ on those fine nodes, which do not overlap with the coarse nodes at the grid interface. This is done by the following formula:

$$\widehat{f_j^f}(x) = a_j(x - x_j)^3 + b_j(x - x_j)^2 + c_j(x - x_j) + d_j \tag{29}$$

The coefficients in Eq. (29) are calculated as follows:

$$\begin{aligned} a_j &= M_{j+1} - \frac{M_j}{6h} \\ b_j &= \frac{M_j}{2} \\ c_j &= (f_{j+1}^f - f_j^f) - \left(\frac{M_{j+1} + 2M_j}{6}\right)h \\ d_j &= f_j^f \end{aligned} \tag{30}$$

where M_j are second order derivatives of the function $\widehat{f_j^f}$ and $h = y_j - y_{j-1}$ measured in the coarse block. The M_j functions are calculated by solving a matrix equation, which leads to a tridiagonal coefficients matrix suitable for the Thomas algorithm, and the natural spline end condition is stipulated where $M_0 = M_n = 0$.

A three-point Lagrangian interpolation scheme is used to calculate the post-collision distribution function on the grid intersection at the desired time in coarse units:

$$\widehat{f_i^f}(t) = \sum_{p=1}^{3}\left[\widehat{f_i^f}(t_p)\Pi_{q=1,p\neq q}^{3}\frac{t - t_q}{t_p - t_q}\right] \tag{31}$$

This leads to the following relation for the temporal interpolation with for example a spacing ratio $m = 4$ and time measured in coarse steps:

$$\begin{aligned} \widehat{f_i^f}(\boldsymbol{t}_{+0.25}) &= -0.09375\widehat{f_i^f}(t_{-1}) + 0.4375\widehat{f_i^f}(t) + 0.65625\widehat{f_i^f}(t_{+1}) \\ \widehat{f_i^f}(\boldsymbol{t}_{+0.5}) &= -0.125\widehat{f_i^f}(t_{-1}) + 0.75\widehat{f_i^f}(t) + 0.375\widehat{f_i^f}(t_{+1}) \\ \widehat{f_i^f}(\boldsymbol{t}_{+0.75}) &= -0.09375\widehat{f_i^f}(t_{-1}) + 0.9375\widehat{f_i^f}(t) + 0.15625\widehat{f_i^f}(t_{+1}) \end{aligned} \tag{32}$$

For simplicity a ratio $m = 2$ was used throughout this work. This required the utilization of only $f_i^f(t_{+0.5})$ from Eq. (32) for the temporal interpolation.

To implement the multi-block concept on the Gunstensen model care should be taken of the collision step which involves the sum $f_i^f(\boldsymbol{x}, t)$ of the two distribution functions $R_i(\boldsymbol{x}, t)$ and $B_i(\boldsymbol{x}, t)$ as it was expressed in Eqs. (10) and (15). Therefore the sum post-collision distribution function $f_i^f(\boldsymbol{x}, t + \delta_t)$ should be used in Eqs. (27) and (28) for the required transfers at the grid interfaces. Since the streaming step in the Gunstensen model occurs with separate post-collision post-segregation distribution functions $\widehat{R_i}(\boldsymbol{x}, t)$ and $\widehat{B_i}(\boldsymbol{x}, t + \delta_i)$, a transfer of the grid interface information from the sum function $f_i^f(\boldsymbol{x}, t + \delta_t)$ to the suspending component function $\widehat{B_i}(\boldsymbol{x}, t + \delta_t)$ is necessary before streaming. This is to ensure that the transfer of information at the interface between the different grids is propagated through the function $\widehat{B_i}(\boldsymbol{x}, t + \delta_t)$ into the fine block. This transfer is not required for the function $\widehat{R_i}(\boldsymbol{x}, t)$ since the physical interface in the proposed model does not cross the grid interface contrary to the experiment of Tolke et al. (2006), and the exchange of information from the various grids is done only at the single phase interface nodes.

The migrating multi-block method's main feature is the exchange of node type at the grid interfaces. For the fluid–fluid interface to be constantly covered by a fine grid while moving, an exchange of boundary coarse nodes with fine nodes downstream of the fluid interface, and alternatively an exchange of fine boundary nodes with coarse nodes upstream of the interface are needed as shown in Fig. 2.

The node type exchange occurs when the distance travelled by the suspended fluid mass center exceeds one coarse lattice spacing in the flow direction. This exchange happens during one coarse time step and it starts with the streaming in the coarse block. Here a distinction should be drawn between the two coarse blocks. The propagation step should start in the downstream coarse block first, because after propagation the coarse distribution function $f_i^{c,d}(\boldsymbol{x}, t)$ is set to zero at the location indicated as old diminishing coarse nodes in Fig. 2, thereby allowing only fine nodes to occupy it. This can be done since the information needed for the propagation has already been passed.

To create two new sets of fine nodes $\widehat{B_i}(\boldsymbol{x}, t)$ on the new grid interface downstream of the suspended fluid, the extrapolation method is used at the location indicated as newly created fine nodes in Fig. 2. For spacing ratio $m \gg 2$, a careful selection of the extrapolation scheme should be done in order to minimize any possible numerical diffusion, since the extrapolation method could become less accurate. Meanwhile, during the same coarse time step, at the grid interface the following functions $(\widehat{f_i^f}(\boldsymbol{x}, t), \widehat{B_i}(\boldsymbol{x}, t), \rho^N(\boldsymbol{x}, t))$ are set to zero

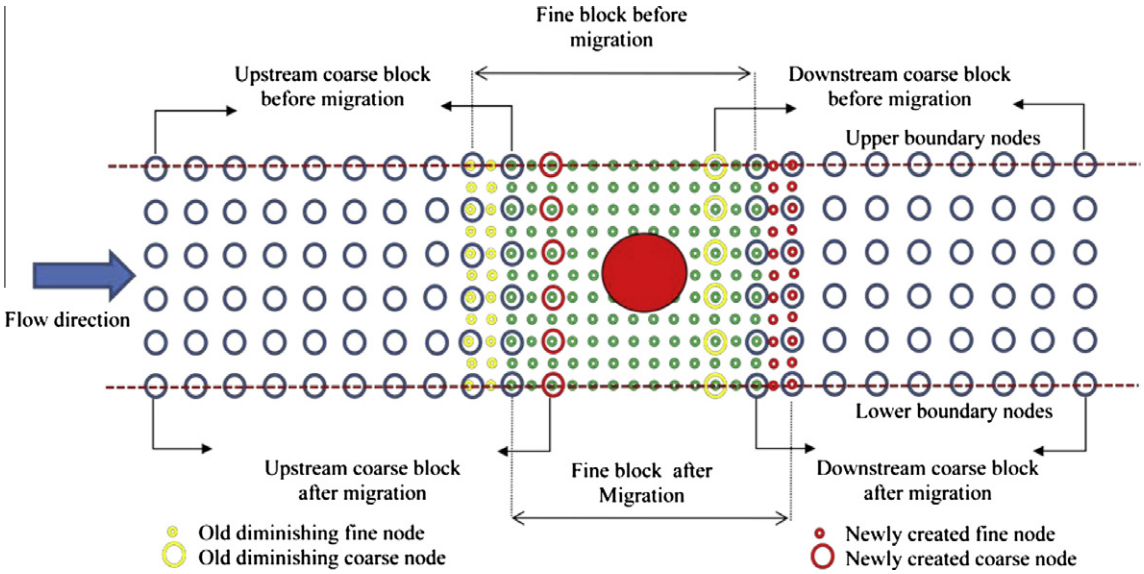

Fig. 2. Illustration of the migrating multi-block LBM domain as it pertains to the multiphase flow simulation used in this paper.

in the locations designated as old diminishing fine nodes in Fig. 2. This will not influence the solution because the information stored in these fine nodes is not required for any subsequent calculations. The propagation in the fine block will not include the vanishing nodes, which position in the domain is now occupied by only coarse nodes. Extrapolation is used again to create a new set of coarse nodes $f_i^{c,u}(\boldsymbol{x},t)$ at the locations indicated as newly created coarse nodes in Fig. 2. This is followed by an immediate transfer of data from the fine node at the new interface to obtain $f_i^{c,u}(\boldsymbol{x},t)$ needed for the propagation in the upstream coarse block. The next step is propagating the upstream coarse block followed by the steps provided in the flow chart of Fig. 3 which resemble the steps of the standard multi-block model.

3. Simulation results and discussion

3.1. Asymmetrically placed cylinder in 2-D channel

To investigate the effects of the migrating block on the numerical solution, an unsteady flow around an asymmetrically placed cylinder in 2D channel was simulated using fixed and migrating multi-block schemes simultaneously. The results were compared with some benchmark cases presented by Schafer and Turek (1996).

The center of the cylinder was located at 4.0 radii from the lower wall, 4.2 radii from the upper wall and 4.0 radii from the inlet as shown in Fig. 4. The fine block covered the whole cylinder, and it was 80 by 164 lattice squares. The total number of nodes in both coarse blocks was 32,800. The ratio between the coarse and the fine grid was $m = 2$. The relaxation times for the fine and the coarse grids were $\tau_f = 0.58$ and $\tau_c = 0.54$, respectively. The average velocity used for the calculation of the Reynolds number was:

$$\overline{U} = \frac{2}{3}U_{(0,\frac{H}{2},t)} \tag{33}$$

where H is the channel height, t is time, and U is the centerline velocity.

The average velocity used for this simulation was $\overline{U} = 0.0666$ lattice units per time step, resulting in a Reynolds number Re = 100. The extrapolation method was enforced on the outlet boundary, and the bounce back condition was implemented on the top and bottom walls as well as on the cylinder surface. The method of Zou and He (1997) was applied on the inlet of the domain using a parabolic velocity profile which was calculated by the following formula:

$$U_{(0,y,t)} = \frac{4U_{(0,\frac{H}{2},t)}y(H-y)}{H^2} \tag{34}$$

Under these conditions was observed leading to periodic vortex shedding. Instantaneous streamlines for the fixed block simulation are shown in Fig. 5a. The Strouhal number defined as $St = \frac{Df}{\overline{U}}$ where D is the cylinder diameter, f is the frequency of separation (the inverse of the period from peak to peak values of the lift coefficient) was $St = 0.293$. This value matched well with the results given by Schafer and Turek (1996).

The same simulation was carried out again with the fine block migrating by one coarse lattice each 5×10^3 coarse time steps. The Strouhal number was calculated as $St = 0.297$. This value agreed well with those given by Schafer and Turek (1996) ($0.295 \leqslant St \leqslant 0.305$). A qualitative comparison between the instantaneous streamlines of Fig. 5b, with the streamlines of Fig. 5a, shows a very marginal difference caused by the moving fine block after five consecutive shifts. The Strouhal numbers in both simulations were derived using the lift coefficient graph of Fig. 6, which was plotted together with the drag coefficients between coarse time steps 3.7×10^4 and 4.0×10^4. The lift and the drag coefficients were calculated using the following formulae, respectively:

$$\begin{aligned} C_L &= \frac{2F_L}{\rho\overline{U}^2D} \\ C_D &= \frac{2F_D}{\rho\overline{U}^2D} \end{aligned} \tag{35}$$

The lift and the drag forces were computed by the following equations, respectively:

$$\begin{aligned} F_L &= -\int_S \left(\mu\frac{\partial v_t}{\partial n}n_x + Pn_y\right)dS \\ F_D &= \int_S \left(\mu\frac{\partial v_t}{\partial n}n_y - Pn_x\right)dS \end{aligned} \tag{36}$$

where F_L was the lift force, F_D the drag force, μ was the fluid dynamic viscosity, P was the local pressure, v_t was the tangential velocity, and n_x, n_y were the x and y components of the normal to the surface of the cylinder S.

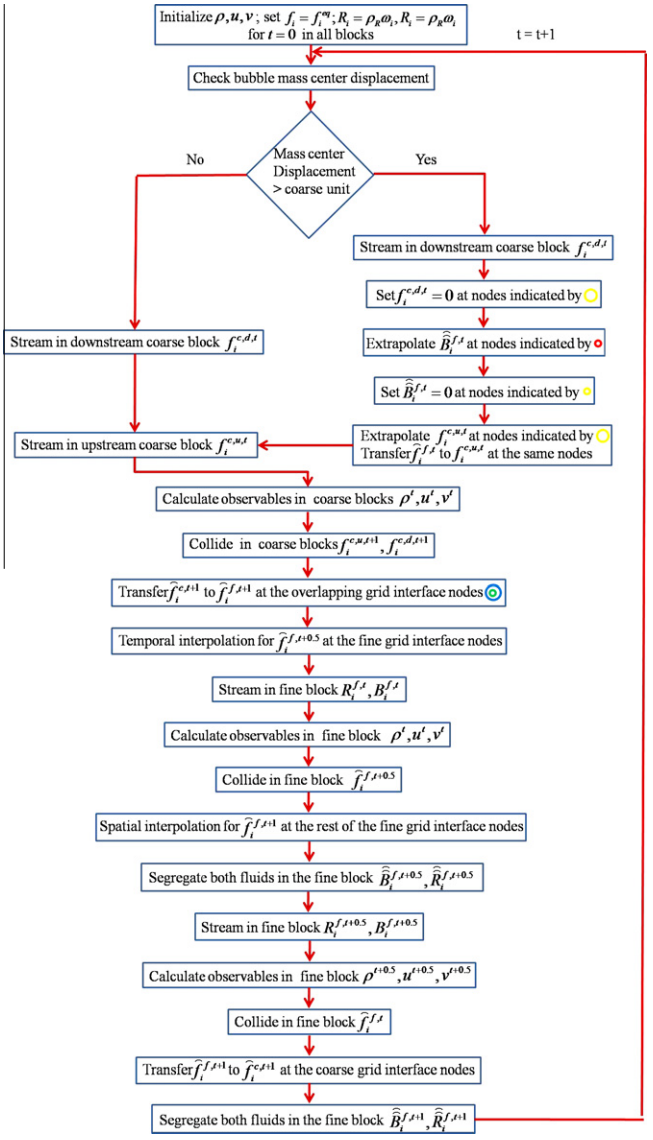

Fig. 3. Flow chart of the migrating multi-block LBM for immiscible mixtures.

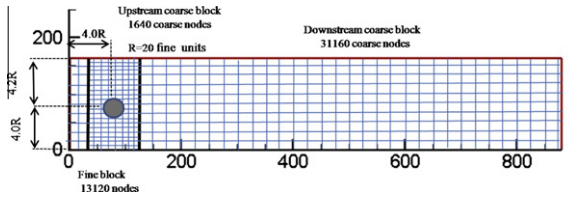

Fig. 4. Migrating multi-block LBM domain for the flow around an asymmetrically placed cylinder in a channel, with the cylinder center location expressed as a function of its radius.

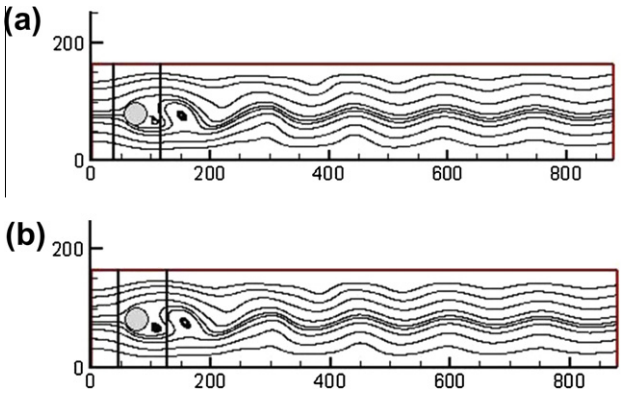

Fig. 5. Instantaneous streamlines of a 2D channel flow over an asymmetrically placed cylinder with Re = 100 time step 2.9×10^4 measured in coarse time units. (a) Fixed multi-block in which the fine block is static having a center coinciding with the cylinder center (b) migrating multi-block in which the fine block migrated in the direction of the flow by one coarse space unit each 5.0×10^3 coarse time steps and having its center advanced by 10 fine space units in the flow direction with respect to the cylinder center.

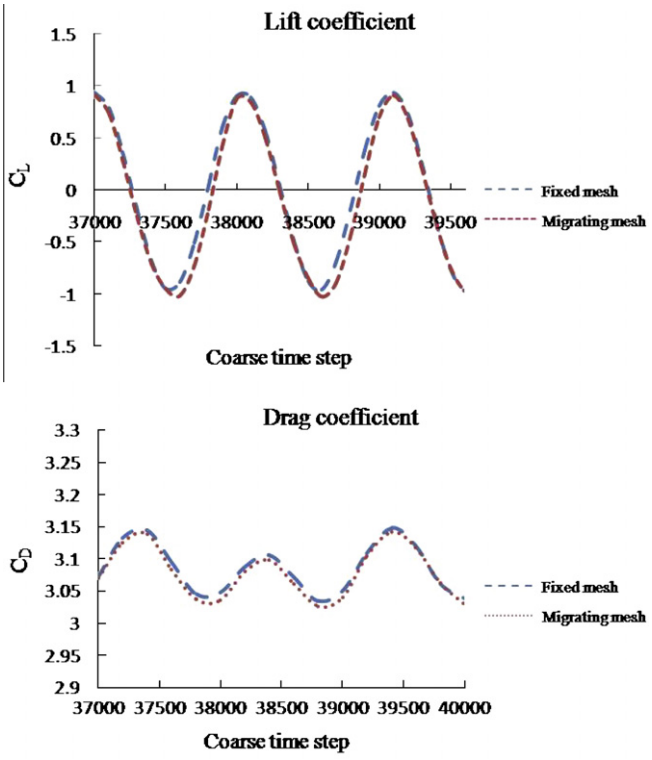

Fig. 6. Lift and drag coefficients for fixed and migrating multi-block cases, calculated for results taken between coarse time steps 3.7×10^4 and 4.0×10^4. A comparison of the two cases indicates that the block migration altered the results just marginally.

The comparison in Fig. 6 shows a reasonable agreement between the two cases and the lift coefficient was not symmetrical with respect to the x axis. This was due to the asymmetrical placement of the cylinder (Yu et al., 2002). The maximum absolute values for the lift coefficient, which was in the negative region, were different in both simulations (0.98 for the fixed block, and 1.03 for the moving block); However both maximum values agreed well with the values given by Schafer and Turek (1996) (0.99–1.01). The drag coefficients were $3.03 \leqslant C_D \leqslant 3.14$ for the fixed block and $3.02 \leqslant C_D \leqslant 3.138$ for the migrating block. Both maximum values were little below the values, which were reported by Schafer and Turek (1996) ($C_{D,\max} = 3.22$–3.24). Fig. 7 shows the vertical velocity contour and the fine block position after the seventh block shift at coarse time step 3.6×10^4.

To test the quality of the data transfer through the grid interfaces and the effects of the fine block migration on the model results, the mass flux and the momentum flux were calculated at the grid interface downstream of the cylinder as shown in Fig. 8. The data were collected from the overlapping coarse and fine nodes of the migrating block at the grid interface, and from the

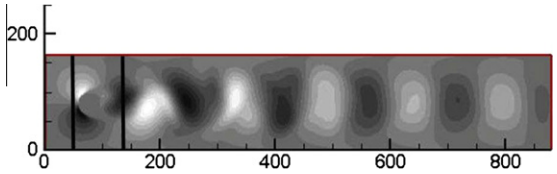

Fig. 7. Vertical velocity contours, and location of the fine block with respect to the cylinder at coarse time step 3.6×10^4.

fixed multi-block nodes which occupied the same spatial locations. The good match between the results of the fine and the coarse block calculations at the migrating block interface was a measure of the used interpolation scheme accuracy, and it showed that the migrating block algorithm did not alter the outcome of the calculations. The slight difference in the y components between the migrating and the fixed block results was due to the difference in the grid size, used for calculating the fluxes in both cases, and also due to the fact that the nodes where the data collection occurred in the fixed multi-block were not grid intersection nodes.

3.2. Lift of a neutrally buoyant drop in parabolic flow

The study of multiphase flows at low to moderate Reynolds and Weber numbers, where the effect of gravity is neglected, is of interest in many applications such as the study of drop suspension in microgravity, and in the study of microfluidics. In very low gravity shear and parabolic flows, the hydrodynamic lift force becomes very important, since it is no longer overshadowed by the buoyancy. The lift force is due to the hydrodynamic interaction of the drop with neighboring boundary (Halliday et al., 2006) or it is caused by a secondary velocity field at the drop surface (Legendre and Magnaudet, 1998).

The goal of this section's simulation was to validate the proposed model by comparing the results for the lateral migration of a 2D neutrally buoyant drop placed near a wall in parabolic flow with other numerical works. The other goal was to assess the quality of the proposed migrating multi-block model results for the lift trajectory and velocity, in comparison with those from the standard Gunstensen model. The approach for the estimation of the shear lift velocity was based on tracking the mass center of the drop. The result was a displacement–time function used for the calculation of the drop lateral velocity. The quality of the measurements depended heavily on the nature of the grid, since the lift force was very small likewise the change in the lateral position of the drop mass center. To minimize the effect of periodicity in the flow direction while attaining the drop equilibrium distance from the wall, a longer channel was required. For a better interface representation it was crucial to refine the grid surrounding the drop. All of this resulted in a high computational cost for the standard LBM meanwhile it provided a good test ground for the proposed migrating multi-block method.

Mortazavi and Tryggvason (2000) carried out a thorough numerical investigation of the drop shear lift in Poiseuille flow. For the case in which the ratio of the drop radius to the channel height was given as $\zeta = 0.125$, the viscosity ratio $\lambda = \frac{\mu_d}{\mu_s} = 8$, the drop Reynolds number $\mathrm{Re}_d = 10.0$ and the Weber number $We = 16$, a normalized equilibrium distance from the wall of $\frac{y_{eq}}{H} \approx 0.30$ was reported.

The drop behavior in parabolic flows is characterized by the following dimensionless numbers. The channel Reynolds number:

$$\mathrm{Re}_{ch} = \frac{\overline{U}H}{\nu} \tag{37}$$

where H is the channel height, $\overline{U}$ is the flow average velocity.

The drop Reynolds number is given by:

$$\mathrm{Re}_d = \frac{\overline{U}d}{\nu} \tag{38}$$

The Weber number is expressed as follows:

$$We = \frac{\rho \overline{U}^2 d}{\alpha} \tag{39}$$

A domain made of 2,87,400 coarse lattice nodes and 168 by 300 fine lattice nodes, covered a drop with diameter $d = 76$ fine lattice units, yielding a ratio $\zeta = d/2H \approx 0.125$. The drop was placed at coordinate (94, 245) measured in fine lattice nodes, the density of both fluids was set to $\rho = 0.514$ and the surface tension parameter to $\alpha = 1.0 \times 10^{-4}$. The relaxation times for the ambient fluid in the fine and coarse grids were set to $\tau_f = 0.646$ and $\tau_c = 0.573$, respectively. The drop relaxation time was $\tau_d = 1.666$ leading to a viscosity ratio $\lambda = 8$. The grid ratio between the coarse and fine the block was $m = 2$. A constant force $|F| = 2.14 \times 10^{-8}$ was used in Eq. (19) to induce a flow with an average velocity $\overline{U} = 0.0064$, a drop Reynolds number $\mathrm{Re}_d = 10.0$ and Weber number $We \approx 16$. The bounce back condition was applied on the upper and the lower walls, and the periodic condition was imposed at the inlet and the outlet boundaries. In the migrating multi-block the following equalities were required in the upstream coarse block after streaming:

$$\begin{aligned} f_i^{c,u}(x_{first}, y, 1) &= f_i^{c,d}(x_{last}, y, 1) \\ f_i^{c,u}(x_{first}, y, 2) &= f_i^{c,d}(x_{last}, y, 2) \\ f_i^{c,u}(x_{first}, y, 8) &= f_i^{c,d}(x_{last}, y, 8) \end{aligned} \tag{40}$$

where $f^{c,u}$ and $f^{c,d}$ are the distribution functions in the upstream and downstream blocks, respectively. x_{first} and x_{last} refer to the first and the last fluid nodes in the horizontal direction, the numbers indicate the lattice directions. In the downstream coarse block the following was applied:

$$\begin{aligned} f_i^{c,d}(x_{last}, y, 4) &= f_i^{c,u}(x_{first}, y, 4) \\ f_i^{c,d}(x_{last}, y, 5) &= f_i^{c,u}(x_{first}, y, 5) \\ f_i^{c,d}(x_{last}, y, 6) &= f_i^{c,u}(x_{first}, y, 6) \end{aligned} \tag{41}$$

The source term of Eq. (19) was augmented by the grid ratio m in the coarse blocks as follows:

$$\phi_i = \omega_i \frac{m}{k_2} \boldsymbol{F} \cdot \boldsymbol{c}_i \tag{42}$$

The drop center of gravity normalized position with respect to the drop axial normalized position is shown in Fig. 9. The migrating multi-block result was compared with the solution of Mortazavi and Tryggvason (2000). The normalized equilibrium distance resulting from the migrating multi-block was $\frac{y_{eq}}{H} \approx 0.31$. The proposed model results were fairly good, in comparison with those of Mortazavi and Tryggvason (2000). The inset in Fig. 9 is for the phase field contours of the drop with superimposed snap shot from the following dimensionless time steps 1.28, 20.48, 30.72, 39.68 and 46.72 respectively. The blue colored blocks in the inset are the superimposed fine migrating blocks, while the green colored are the coarse blocks.

To compare the results of the proposed model with those of the standard LBM, the same flow condition and geometric settings were used for a domain consisting of 2000 by 300 lattice squares to avoid excessive computations in the standard LBM. The equivalent domain for the migrating block scheme consisted of 1,37,400 coarse lattice nodes and 168 by 300 fine lattice nodes. The drop was placed at coordinate (94, 248) measured in fine lattice nodes.

A dimensionless approach was used for the analysis of the results. H was selected as a characteristic length, $U_0 = \frac{3}{2}\overline{U}$ the undisturbed centerline flow velocity, as characteristic velocity, and the inverse shearing strain rate $\dot{\gamma}^{-1} = \frac{H}{2U_0}$ as characteristic time. The shear rate was calculated at the vertical position $3H/4$ since this position was representative to the equilibrium point in the drop lift

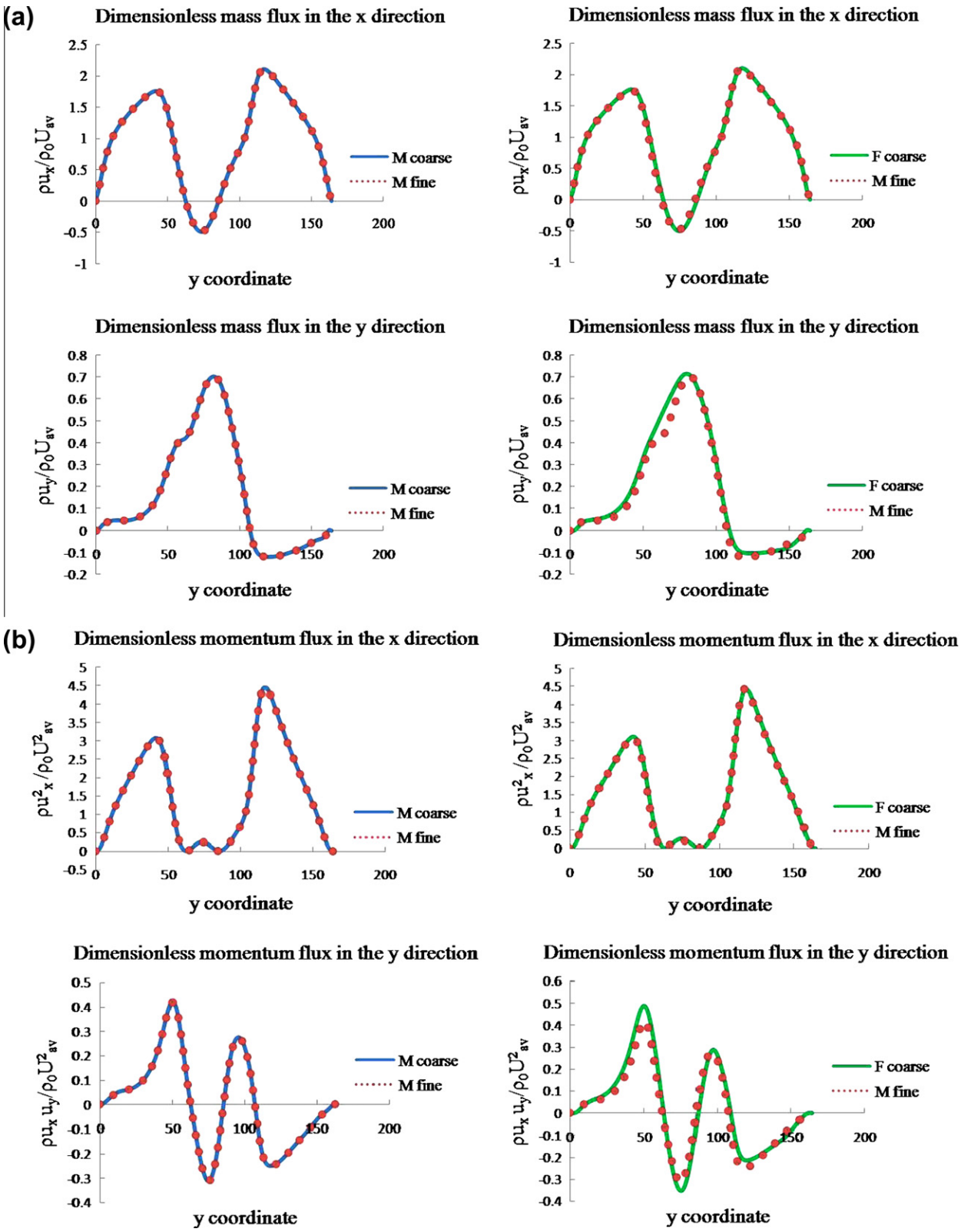

Fig. 8. Graphs for the dimensionless mass flux in the *x* and *y* directions (a) and dimensionless momentum flux in the *x* and *y* directions (b) with respect to the *y* coordinates at coarse time step 3.5×10^4, calculated for checking the quality of the data transfer through the grid interface between the fine bock and the downstream coarse block in the migrating multi-block model. Comparison between the results of the moving fine grid interface's nodes with those collected from the fixed multi-block coarse nodes which occupy the same locations. M and F in the figure stand for moving and fixed blocks, respectively.

activity space. The normalized fluid average velocities and the normalized displacements of the drop mass center in the flow direction versus dimensionless time from the two simulations are shown in Fig. 10. The lateral displacements normalized by the channel width, versus the dimensionless time from both simulations are shown in Fig. 11. The lift velocities were calculated from

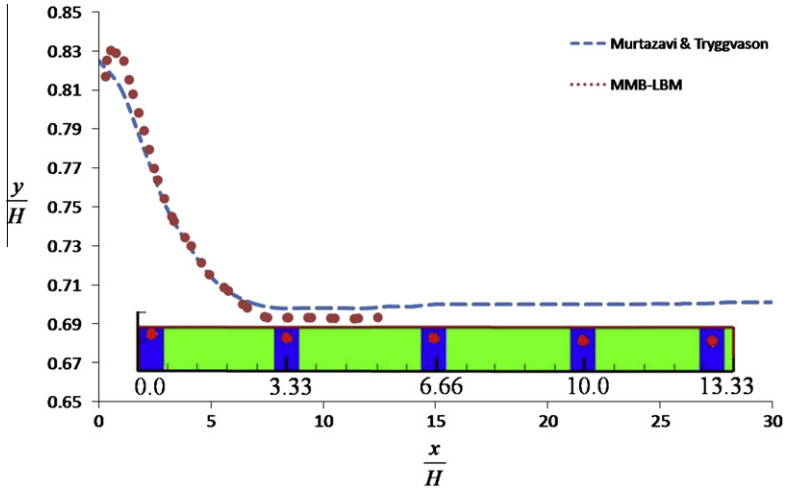

Fig. 9. Drop mass center normalized lateral displacement by the migrating multi-block LBM compared with the solution of Mortazavi and Tryggvason (2000) for the case with $Re_d = 10.0$, $We = 16$, $\lambda = 8$, and $\zeta = 0.125$. No further data was provided for $x/H > 13.3$ since the drop reached the end of the domain (4000×300) in the MMB model measured in fine lattice. The inset in the figure is for the phase field contours of the drop with superimposed snap shots from the following dimensionless time steps 1.28, 20.48, 30.72, 39.68 and 46.72 respectively. The blue colored blocks in the inset are the superimposed fine migrating blocks, while the green colored are the coarse blocks. (For interpretation of the references to colour in this figure legend, the reader is referred to the web version of this article.)

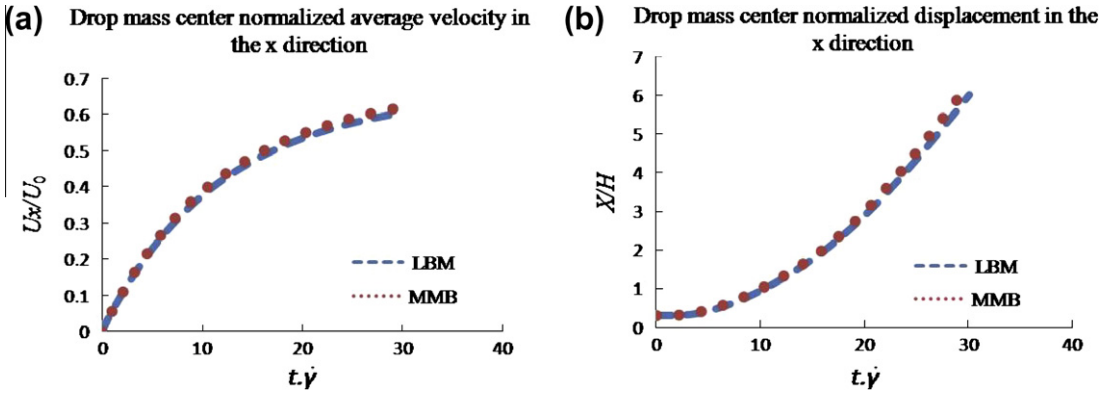

Fig. 10. Normalized fluid average velocities in the x direction (a), and drop mass center normalized horizontal displacements in the x direction (b), for both the migrating block and the standard Gunstensen model versus dimensionless time.

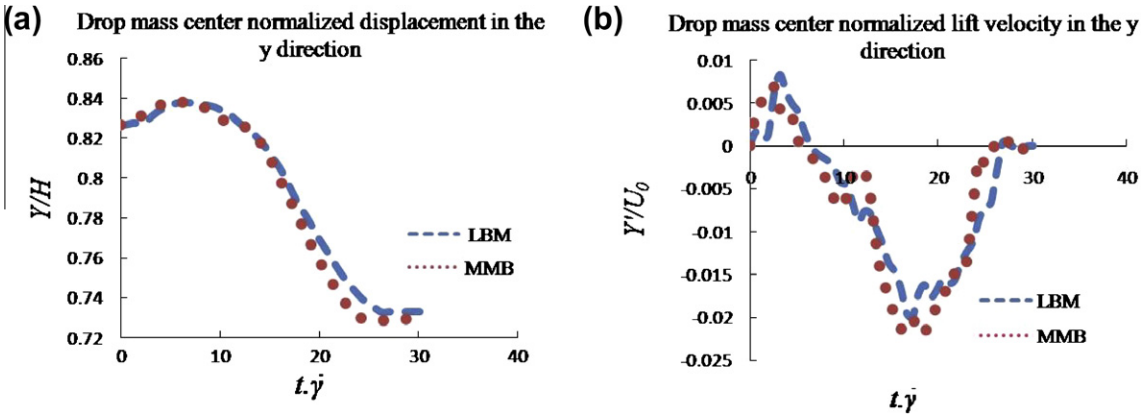

Fig. 11. Normalized displacement of the drop mass center in the y direction (a) for the migrating block and the standard LBM measured with respect to dimensionless time. Normalized lift velocity (b) in the y direction for the migrating block and the standard LBM calculated with respect to the dimensionless time.

the lift displacement–time data as time derivative by a finite difference scheme with second order accuracy then were normalized by the centerline flow velocity as shown in Fig. 11.

It was clear from Fig. 11 that the velocities observed at $t\dot{\gamma} < 7$ should be neglected due to the drop tilt during the initialization of the simulations, and that the drop's lift velocity is an order of

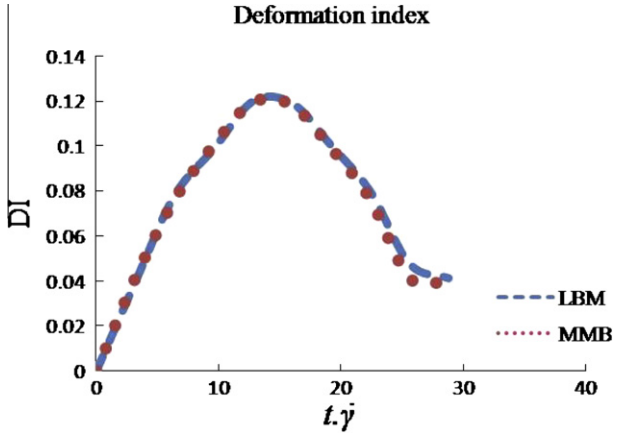

Fig. 12. Deformation index of the drops from both the standard LBM and the migrating multi-block calculated with respect to the dimensionless time.

magnitude smaller than its translational velocity. The same was extracted in the work of Sukumaran and Siefert (2001) who studied the lift of the near-wall neutrally buoyant vesicles in shear flow. The distance from the top wall at dimensionless time step $t\dot{\gamma} = 28.8$ for the standard LBM was $\frac{y}{H} = 0.2733$ versus $\frac{y}{H} = 0.2728$ for the migrating block.

The deformation index $DI = \frac{(a-b)}{(a+b)}$, where a is the drop major axis and b is the drop minor axis, varied between the values $0 \leqslant DI \leqslant 0.12$ during the simulations as shown in Fig. 12. The reduction in the DI associated with time was due to the reduction in the viscous stress, when the drop drifted away from the wall leading to a reduced DI.

Cox (1969) proposed a theoretical formula for the calculation of the drop deformation in a general time-dependent fluid flow with a range of capillary numbers and viscosity ratios. The time dependence of the DI was through a decaying exponential function which led after long time (steady state) to the following relationship:

$$DI = \frac{5(19\lambda + 16)}{4(\lambda + 1)\sqrt{\left(\frac{20}{Ca}\right)^2 + (19\lambda)^2}} \tag{43}$$

where $Ca = \mu_s \dot{\gamma} d/2\alpha$ is the capillary number. The strain rate used in the calculation of this work's capillary number was locally defined by $\dot{\gamma}(y) = \left|\frac{8U_0}{H^2}\left(\frac{H}{2} - y\right)\right|$. The deformation index calculated by Eq. (43) yielded $DI = 0.151$ for the dimensionless time step $\dot{\gamma}t = 12.8$ and the calculated capillary number $Ca = 0.78$. The dimensionless mass center location was $\frac{y}{H} = 0.824$, which corresponded to the location where the simulation results led to the highest value $DI = 0.12$ as shown in Fig. 12. The difference between the measured and the calculated deformation indices could be resulting from the transient nature of the drop deformation under the shear lift as measured from the simulation, compared to the steady state deformation described by Eq. (43).

Fig. 13 presents the phase field contours, with the various positions of the drop generated by super-imposing consecutive snap shots taken at different time steps.

To analyze the computational time advantage of the proposed model the following formula was introduced:

$$G = m\frac{N_x N_y}{mL_x N_y + \frac{1}{m^2}(N_x - L_x)N_y} \tag{44}$$

where N_x and N_y are the domain length and width measured in fine grids spacing respectively, and L_x is the length of the fine block. Eq. (44) was based on the idea that for the calculation of one time step in the coarse blocks expressed in fine lattice units as $(N_x - L_x)N_y/m^2$,

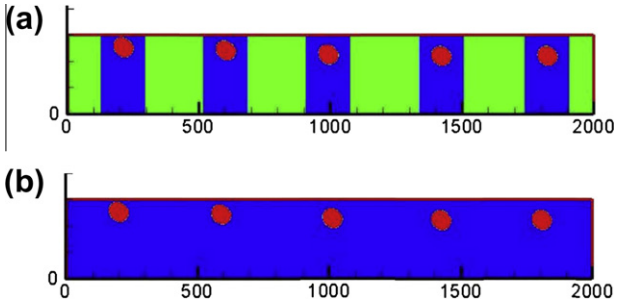

Fig. 13. Phase field contour for five consecutive snap shots taken at different time steps and superimposed in the figure. The blue blocks are fine, and the green blocks are coarse: (a) migrating multi-block and (b) standard LBM. (For interpretation of the references to colour in this figure legend, the reader is referred to the web version of this article.)

there is a need for m time steps in the fine block having dimensions $L_x N_y$ and in the standard LBM with dimensions $N_x N_y$, respectively. Eq. (44) is applicable only for 2D models, with the fine block covering the entire width. For the current simulation the formula leads to a time gain $G = 5.04$. This was also confirmed by comparing the computational time required for the simulations using the standard Gunstensen model and the proposed migrating multi-block method simultaneously. Using DELL Precision 490 workstation, one time step in the standard model required 0.516 s for execution, while the time needed for the same time step in the migrating multi-block was 0.108 s leading to $G = \frac{t_{st}}{t_{mmb}} = 4.77$. The difference between the calculated and the measured computational time gain could be used to evaluate the code level of efficiency.

4. Conclusion

A 2D multiphase LBM, with the migrating multi-block method was presented in this paper. The advantage of this model is the simplicity of its algorithm and the ability to refine the mesh in regions, where a better interface resolution is required, without excessive computational cost and loss of accuracy. The method was used with a lattice spacing ratio of $m = 2$ which is not explicit. Higher values can be used, provided that numerical diffusion is well controlled. Expansion of the model into three dimensions will be the focus of a future work since time saving in 3D models is more significant.

Acknowledgments

This study was partially supported by a grant of the Korea Healthcare technology R&D Project, Ministry for Health, Welfare & Family Affairs, Republic of Korea. (Grant Number: A085136) and by Basic Science Research Program through the National Research Foundation of Korea (NRF) funded by the Ministry of Education, Science and Technology (Grant number: 2010-0007113).

References

Chen, H., Chen, S., Matthews, W.H., 1992. Recovery of the Navier–Stokes equations using lattice-gas Boltzmann method. Phys. Rev. A 45, 5339–5342.
Cox, R.G., 1969. The deformation of a drop in a general time-dependent fluid flow. J. Fluid Mech. 37, 601–623.
D'Ortona, U., Salin, D., Cieplak, M., Rybka, R., Banavar, J., 1995. Two-color nonlinear Boltzmann cellular automata: surface tension and wetting. Phys. Rev. E. 51, 3718–3728.
Dupin, M., Halliday, I., Care, C., 2003. Multi-component lattice Boltzmann equation for mesoscale blood flow. J. Phys. A. Math. Gen. 36, 8517–8534.
Dupin, M., Halliday, I., Care, C., 2005. A multi-component lattice Boltzmann scheme: towards the mesoscale simulation of blood flow. Med. Eng. Phys. 28, 13–18.
Dupin, M., Halliday, I., Care, C., Alboul, L., 2007. Modeling of the flow of dense suspension of deformable particles in three dimensions. Phys. Rev. E 75, 066707-1–066707-17.

Fillipova, O., Hanel, D., 1998. Grid refinement for lattice-BGK models. J. Comput. Phys. 147, 219–228.
Gunstensen, A., Rothman, D., Zaleski, S., Zanetti, G., 1991. Lattice Boltzmann model of immiscible fluids. Phys. Rev. A. 43, 4320–4327.
Guo, Z., Sheng, C., Wang, N., 2000. Lattice BGK model for incompressible Navier–Stokes equation. J. Comput. Phys. 165, 288–306.
Guo, Z., Sheng, C., Shi, B., 2002. Discrete lattice Boltzmann effects on the forcing term in the lattice Boltzmann method. Phys. Rev. E 65, 046308-1–046308-6.
Halliday, I., Hollis, A., Care, C., 2006. Improved simulation of drop dynamics in a shear flow at low Reynolds number and capillary number. Phys. Rev. E 73, 056708-1–056708-11.
Halliday, I., Hollis, A., Care, C., 2007. Lattice Boltzmann algorithm for continuum multicomponent flow. Phys. Rev. E 76, 026708-1–026708-13.
He, X., Doolen, G., 1997. Lattice Boltzmann method on curvilinear coordinates system: flow around a circular cylinder. J. Comput. Phys. 134, 306–315.
He, X., Luo, L., Dembo, M., 1996. Some progress in lattice Boltzmann method. Nonuniform mesh grids. J. Comput. Phys. 129, 357–363.
Huang, D., Lee, T.S., Shu, C., 2006. Hybrid lattice Boltzmann finite-difference simulation of axisymmetric swirling and rotating flows. Int. J. Numer. Methods Fluids 53, 1707–1726.
Imamura, T., Suzuki, K., Nakamura, T., Yshida, M., 2005. Acceleration of steady-state lattice Boltzmann simulations on non-uniform mesh using local time step method. J. Comput. Phys. 202, 645–663.
Kandhai, D., Soll, W., Chen, S., Hoekstra, A., Sloot, P., 2000. Finite-difference lattice-BGK methods on nested grids. Comput. Phys. Commun. 129, 100–109.
Legendre, D., Magnaudet, J., 1998. The lift force on spherical bubble in a viscous linear shear flow. J. Fluid Mech. 368, 81–126.
Li, Y., LeBoeuf, E., Basu, P.K., 2005. Least-squares finite-element scheme for the lattice Boltzmann method on an unstructured mesh. Phys. Rev. E 72, 046711-1–046711-11.
Lin, C., Lai, Y., 2000. Lattice Boltzmann method on composite grids. Phys. Rev. E 62, 2219–2225.
Lishchuk, S., Care, C., Halliday, I., 2003. Lattice Boltzmann algorithm for surface tension with greatly reduced microcurrents. Phys. Rev. E 67, 036701-1–036701-5.
Liu, D., Zhou, J., Burrows, R., 2009. Multi-block lattice Boltzmann simulations of subcritical flow in open channel junctions. Comput. Fluids 38, 1108–1117.
Mortazavi, S., Tryggvason, G., 2000. A numerical study of the motion of drops in Poiseuille flow. Part 1. Lateral migration of one drop. J. Fluid Mech. 411, 325–350.
Ozawa, T., Tanahashi, T., 2005. CIVA and ANR method for discrete Boltzmann equation. JSME Int. J. 48, 229–234.
Reis, T., Philip, T., 2007. Lattice Boltzmann model for simulating immiscible two-phase flows. J. Phys. A: Math. Theor. 40, 4033–4053.
Schafer, M., Turek, S., 1996. Benchmark computations of laminar flow around a cylinder. Notes Numer. Fluid Mech. 52, 547–566.
Shu, C., Chew, Y.T., Niu, X.D., 2001. Least-squares-based lattice Boltzmann method: a meshless approach for simulation of flows with complex geometry. Phys. Rev. E 64, 045701-1–045701-4.
Sukumaran, S., Siefert, U., 2001. Influence of shear flow on vesicles near a wall: a numerical study. Phys. Rev. E 64, 011916-1–011916-11.
Tolke, J., Freudiger, S., Krafczyk, M., 2006. An adaptive scheme using hierarchical grids for lattice Boltzmann multi-phase flow simulations. Comput. Fluids 35, 820–830.
van der Sman, D., 2004. Diffusion on unstructured triangular grids using lattice Boltzmann. Future Gen. Comput. Syst. 20, 965–971.
Yu, D., Girimaji, S., 2006. Multi-block lattice Boltzmann method: extension to 3D and validation in turbulence. Physica A 362, 118–124.
Yu, D., Mei, R., Shyy, W., 2002. A multi-block lattice Boltzmann method for viscous fluid flows. Int. J. Numer. Methods Fluids 39, 99–120.
Zou, Q., He, X., 1997. On pressure and velocity boundary conditions for the lattice Boltzmann BGK model. Phys. Fluids 9, 1591–1598.